Journal of Membrane Science 620 (2021) 118768

Contents lists available at ScienceDirect

Journal of Membrane Science

journal homepage: http://www.elsevier.com/locate/memsci

Superhydrophobic-omniphobic membrane with anti-deformable pores for membrane distillation with excellent wetting resistance

Zhigao Zhu [a], Lingling Zhong [b], Thomas Horseman [c], Zhiyuan Liu [d], Gaofeng Zeng [e], Zhenyu Li [f], Shihong Lin [c,g], Wei Wang [b,*]

[a] Key Laboratory of New Membrane Materials, Ministry of Industry and Information Technology, School of Environment and Biological Engineering, Nanjing University of Science and Technology, Nanjing, 210094, China
[b] State Key Laboratory of Urban Water Resource and Environment, School of Environment, Harbin Institute of Technology, Harbin, 150090, China
[c] Department of Chemical and Biomolecular Engineering, Vanderbilt University, Nashville, TN, 37235, United States
[d] Shenzhen Institutes of Advanced Technology, Chinese Academy of Sciences, Shenzhen, 518055, China
[e] CAS Key Laboratory of Low-Carbon Conversion Science and Engineering, Shanghai Advanced Research Institute, Chinese Academy of Sciences, Shanghai, 201210, China
[f] Chengdu Evermaterials Co., Ltd, Chengdu, Sichuan, 610500, China
[g] Department of Civil and Environmental Engineering, Vanderbilt University, Nashville, TN, 37235-1831, United States

ARTICLE INFO

Keywords:
Superhydrophobic-omniphobic surface
Anti-deformable pores
Membrane distillation
Membrane scaling
Electrospinning

ABSTRACT

Wetting induced by salt-scaling and surfactants is the Achilles heel of membrane distillation, especially for concentration of high salinity wastewater. Herein, we rationally developed a membrane with robust wetting resistance by integrating superhydrophobic-omniphobic surface and anti-deformable pores into one system. The membrane was first developed by electrospinning, which was then modified with surface roughness, and followed by coating of polydimethylsiloxane to weld the intersecting fibers and fluoroalkylsilane to lower the membrane surface energy. The product exhibits excellent wetting resistance when concentrating the high salinity NaCl solution from 20 to 38 wt% (saturation condition), the simulated reverse osmosis concentrated water, the gypsum and the low-surface-tension high salinity wastewater. Moreover, the mechanism of membrane wetting resistance was also systematically discussed based on the experiment and computer simulation. It reveals that the superhydrophobic-omniphobic surface could stabilize the surface-bound air layer chemically, thus reducing the contact of crystals and surfactant with the membrane surface. Simultaneously, the anti-deformable pore also helps it overcome the asymmetrical hydraulic disturbance on enlarging membrane pore size, thus stabilizes the surface-bound air layer structurally. The presented development will provide a platform to understand and achieve wetting and scaling inhibition MD membrane for high salinity wastewater treatment.

1. Introduction

High salinity wastewater generated from the petrochemical, steel, mining, and seawater desalination industries takes a heavy toll on the global environment and human health [1–4]. Conventional methods for treating high salinity wastewaters include thermal and membrane desalination technologies [5–8]. However, thermal desalination technologies (e.g., multi-effect distillation and multistage flash evaporation) generally require high-grade heat energy as a driving force and also suffer from corrosion when immersed in salt solutions [9–11]. While the most commonly membrane desalination technologies (e.g., reverse/-forward osmosis and nanofiltration membranes) cannot concentrate the high salinity wastewater due to its high osmotic pressure and high propensity for membrane fouling [12,13]. Membrane distillation (MD), a membrane-based thermal desalination process, has emerged as a promising solution for concentrating high salinity wastewaters. MD has the advantages of using low-grade waste heat to produce high-quality water with high recovery from highly saline feed water [14,15]. Besides, the common advantages of membrane processes, such as system compactness and modularity, also render MD attractive as technology for decentralized management of high-salinity wastewater.

Nevertheless, a significant challenge when using MD for treating high-salinity wastewaters is pore wetting, which renders the hydrophobic membranes that are typically used in MD processes ineffective

* Corresponding author.
E-mail address: wangweirs@hit.edu.cn (W. Wang).

https://doi.org/10.1016/j.memsci.2020.118768
Received 26 June 2020; Received in revised form 17 September 2020; Accepted 21 September 2020
Available online 22 September 2020

for desalination [16]. On the one hand, dissolved salts in the feed water eventually precipitate and accumulate on the membrane surface, a phenomenon known as membrane scaling. As the scaling crystals are imbedded into the surface pores of the hydrophobic membranes, crystallization and oriented growth processes cause crystals to penetrate into the membrane matrix which deforms the membrane pores and eventually results in pore wetting [7,17,18]. On the other hand, the low surface-tension amphiphilic contaminants, such as surfactants, in the feed water can also result in pore wetting via lowering the surface tension of the feed solution and saturating the hydrophobic pore surface with surfactants [19–22]. These challenges can be addressed by developing MD membranes with special wetting properties. Specifically, it has been demonstrated that the superhydrophobic membranes with the surface water contact angle of greater than 150° can mitigate mineral scaling and pore wetting, while the omniphobic membranes with low-surface-tension of lower than 10 mN m^{-1} can effectively mitigate membrane pore wetting induced by surfactants [23,24]. However, simultaneous wetting resistance, e.g., the simultaneous mitigation of wetting induced by mineral scaling and by the addition of surfactants has rarely been reported.

Beside intrinsic surface wettability, the pore structure of the MD membrane is another crucial factor determining the durability and desalination performance of MD [25,26]. Fibrous membranes fabricated using electrospinning have been widely used in MD due to their high porosity, low tortuosity, and therefore resulting higher water flux [27–30]. However, fibrous MD membranes with interconnected pores generally suffer from membrane wetting more readily as compared with MD membranes made using other methods. This instability of fibrous MD membranes can be attributed to the asymmetrical hydraulic perturbance on the two sides of the membrane that leads to deformation of pores formed via stacking of random fibers with weak interactions (Fig. 1a) [31,32]. In comparison, conventional MD membrane formed via phase inversion is more resistant to pore wetting induced by hydraulic perturbance due to the more robust porous structure of membrane formed via phase inversion, even though these membranes usually have lower flux as compared to fibrous MD membranes (Fig. 1b) [4,33]. Developing strategies to enhance the robustness of fibrous MD membranes is critical to taking advantage of their beneficial high-flux characteristics without sacrificing salt rejection.

In this study, we develop a novel superhydrophobic-omniphobic fibrous MD membrane with pore structure that is robust to hydraulic perturbation (Fig. 1c). The robust superhydrophobic-omniphobic (RSHO) MD membrane is constructed by electrospinning of polyimide fibers followed by membrane roughness construction and inter-fiber crosslinking and fluorination (Fig. 1d). The wetting resistance of the RSHO membrane is systematically evaluated against scaling and surfactant-induced pore wetting. We also discuss the mechanism of wetting resistance with the RSHO membrane and the importance of the synergistic effect of wetting property and pore stability in imparting robust wetting resistance in MD against different wetting mechanisms.

2. Materials and methods

2.1. Materials

The electrospun polyimide reference membrane was provided by Jiangxi Advanced Nanofiber S&T Co., Ltd. The commercial hydrophobic polyvinylidene fluoride microfiltration membrane denoted as C-membrane was purchased from Merck Millipore. Trimethoxy (heptadecafluorotetrahydrodecyl)-triethoxysilane (17-FAS) and sodium dodecylbenzene sulfonate (SDBS) were purchased from Aladdin Chemical Regent Company. Silica nanoparticles (Ludox SM, 30 wt%) with an average diameter of 30 nm were purchased from Sigma-Aldrich Company. Dopamine (DA), polyethylenimine (PEI, M_w = 600), tris

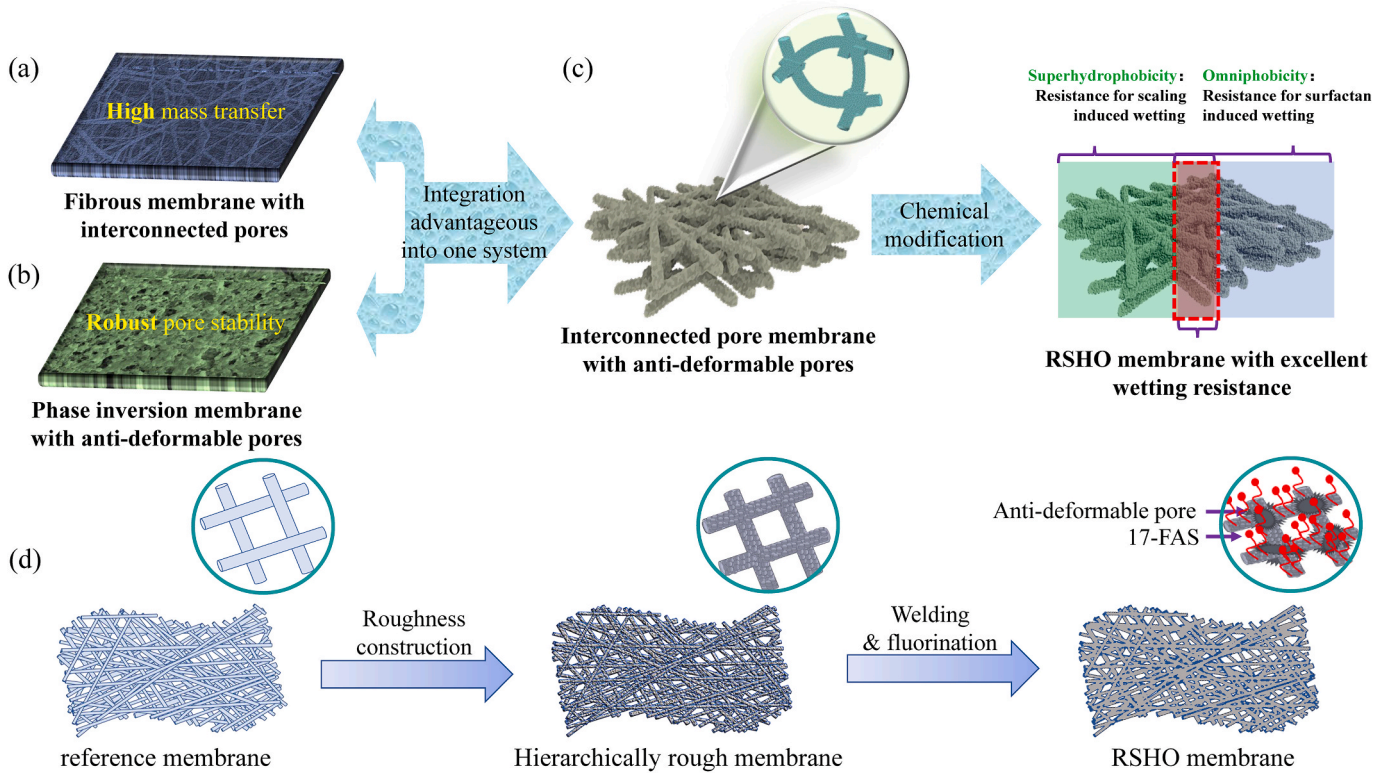

Fig. 1. Schematic illustrating (a) the fibrous membrane with interconnected pores for high mass transfer and (b) phase inversion membrane with anti-deformable pores for robust pore stability. (c) Schematic illustrating the integration of the interconnected pores of the fibrous membrane with the stabilized-pore microfiltration membrane into one system in combination with chemical modification for wetting resistance. (d) Schematic procedures for the fabrication of the RSHO membrane with excellent wetting resistance for concentrating the high salinity wastewaters.

(hydroxymethyl)aminomethane hydrochloride (Tris-HCl), sodium chloride (NaCl) and n-hexane were purchased from Shanghai Runjie Chemical Reagent Company, China. Polydimethylsiloxane (PDMS) precursor composed of the dimethylsiloxane (Sylgard 186) and the curing agent was purchased from Dow Corning Co. Sodium chloride (NaCl), calcium chloride ($CaCl_2$), potassium chloride (KCl), magnesium chloride ($MgCl_2$), magnesium sulfate ($MgSO_4$), and calcium sulfate ($CaSO_4$) were purchased from Tianjin Benchmark Chemical Reagent Company, China. The crude oil and the soya-bean oil were obtained from the fifth Daqing Oil Production Factory and Jiusan Oils & Grains Industries Group Co., Ltd, respectively. The lubricating oil (L-DVB) was purchased from Japan Mitsubishi Heavy Industries Co., Ltd. All chemicals were used as received without further purification.

2.2. Fabrication of the RSHO membrane

First, positive surface charge was imparted on the reference membrane by immersing it in 10 mM tris-buffer solution with 2 mg mL^{-1} DA and 6 mg mL^{-1} PEI and stirring at room temperature for 24 h. The PDA/PEI-modified membrane was rinsed thoroughly with deionized water at least three times and dried at 60 °C for 1 h. The PDA/PEI-modified membrane was then immersed in ~1 mM acetate buffer (pH adjusted to ~4.5) with 0.2 wt% silica nanoparticles for 12 h to electrostatically adsorb silica nanoparticles for the assembly of a hierarchically rough fiber surface. After, the surface was rinsed with deionized water and dried at 60 °C for 1 h [34]. The silica nanoparticle-modified membrane was then soaked in an n-hexane solution with 1 wt% 17-FAS and 1 wt% PDMS precursor for 12 h. Finally, the membrane was heated at 120 °C for 2 h to weld the fluorinated fibers and was denoted as the RSHO membrane for the remainder of the study. Two additional membranes were fabricated with the reference membrane as the substrate to elucidate the effect of the individual fabrication steps on the RSHO membrane wetting resistance. One membrane was modified by single-component PDMS (denoted as the Anti-dp membrane) and the other membrane was modified with silica nanoparticles and fluorinated with 17-FAS (denoted as the SH-Omni membrane).

2.3. Membrane characterization

The morphologies of membranes were observed by a field emission scanning electron microscope (FE-SEM) (Zeiss, Sigma 500). The surface wettability of the membranes was quantified via static water contact angle measurement with a contact angle goniometer (Kino SL200B). The air permeability of membranes was measured by a Frazier air permeability tester (YG461E, NBFY Co., Ltd., China), the mechanical properties were quantified via tensile tester (XQ-1C, Shanghai New Fiber Instrument Co., Ltd., China), and the liquid entry pressure was measured using a capillary flow porometer (POROLUX 1000, Germany).

2.4. Membrane performance experiments

The anti-wetting performance of the membranes was compared using a lab-scale direct contact membrane distillation (DCMD) device with the membrane area fixed at 9 cm^2. The temperature of the feed solution was maintained at 55 °C and the temperature of the distillate solution was maintained at 20 °C. The flow rates of the feed and distillate streams were fixed at 100 mL min^{-1} (~9.21 cm s^{-1} in our MD module). To compare the resistance to scale-induced wetting between phase-inversion membranes and electrospun fibrous membranes, feed solutions of 3.5, 10, and 20 wt% NaCl concentrations were systematically studied. To compare the resistance to surfactant-induced wetting, the membranes were subjected to a feed solution with 0.1 mM SDBS and 20 wt% NaCl. To investigate the resistance to scale-induced wetting and abilities to effectively concentrate industrially relevant high-salinity wastewaters between the fibrous membrane fabrication steps, the membranes were subjected to three model feed solutions: one with gypsum (14 mM $CaCl_2$ and 14 mM Na_2SO_4), one with 1.5 wt% $CaCl_2$, and one with reverse osmosis brine with 32.61 g L^{-1} NaCl, 1.03 g L^{-1} KCl, 4.52 g L^{-1} $MgCl_2$, 2.91 g L^{-1} $MgSO_4$ and 1.80 g L^{-1} $CaSO_4$ was used [34].

2.5. Simulation experiment

The ABAQUS software was used to simulate the impact force of water flow and determine its effect on membrane pore deformation. In the simulation experiment, the Young's modulus of PDMS welded fibers at their junction was set to 2 MPa, while the network without PDMS welding was taken as the reference with Young's modulus of 20 kPa because of its weak electrostatic interaction. The pressure applied to the surface of the fiber is uniform with one magnitude in the software and the pressure is the same as these two models.

3. Results and discussion

3.1. Membrane physical and wetting properties

Wetting of MD membranes can be segmented into two main routes: (1) wetting induced via hydraulic perturbance and (2) wetting induced via feed species, e.g., scalants, surfactants, and low surface tension water miscible liquids [35]. For MD membranes, the resistance to wetting via hydraulic perturbance is generally associated with membrane physical properties such as surface morphology, pore structure, and mechanical properties [36–38]. As shown in Fig. S1a, the C-membrane, fabricated via phase inversion, exhibits an anti-deformable pore structure with an average pore diameter of about 0.30 μm where the reference membrane, fabricated by electrospinning, exhibits interconnected pores with an average fiber diameter of 0.92 μm but a loose non-woven fabric structure (Fig. 2a). Interestingly, after crosslinking the reference membrane with PDMS (Anti-dp), the loose non-woven fibers were welded at their cross-points without apparent pore blockage (Fig. 2b), exhibiting a similar pore structure to the C-membrane.

Apart from the pore structure, the membrane surface morphology plays a critical role in preventing membrane wetting. Direct contact between the membrane surface and the high-salinity water can be avoided by establishing a surface that is both rough and of low-surface energy, which is required to achieve a Cassie-Baxter wetting state [23,39,40]. The SH-Omni membrane exhibits rough surface morphology with silica nanoparticles with an average diameter of about 30 nm uniformly (Fig. 2c and Fig. S2) and stablely distributed along the fiber axis as demonstrated in our previous study [34]. Surprisingly, owing to the viscosity characteristic of dimethylsiloxane (DMS) solution, the DMS and the curing agent can easily adhere to the fiber surface and then fill the gap between the nanoparticles after welding and fluorination, which not only can stabilize the membrane pores but also enhance the stability of nanoparticles on the fiber surface as shown in Fig. 2d.

Liquid entry pressure (LEP) represents the membrane's ability to resist wetting via hydraulic perturbance and is inversely related the membrane pore size, but also depends on the membranes ability to resist pore deformation under stress. As demonstrated in Fig. S1b and 2a, the large pore diameter and loose non-woven nature of the reference fibrous membrane explains the inferior LEP (~35 KPa) relative to the C-membrane (~170 KPa) and thus relative ease in which conventional fibrous membranes are wetted due to physical perturbation compared to the smaller and more robust pore structure in membranes fabricated via phase inversion (Fig. 2e). While fibrous membrane's resistance to wetting due to physical perturbance is generally inferior to that of membranes fabricated via phase inversion, fibrous membranes exhibit superior flux due to their larger porosity, and thus, permeability to water vapor. For example, the air permeability, which represents the ease of gas transport, such as water vapor, through the membrane was measured to be 1.51 mm s^{-1} for the C-membrane while that of the reference fibrous membrane was 13.72 mm s^{-1}. Interestingly, welding

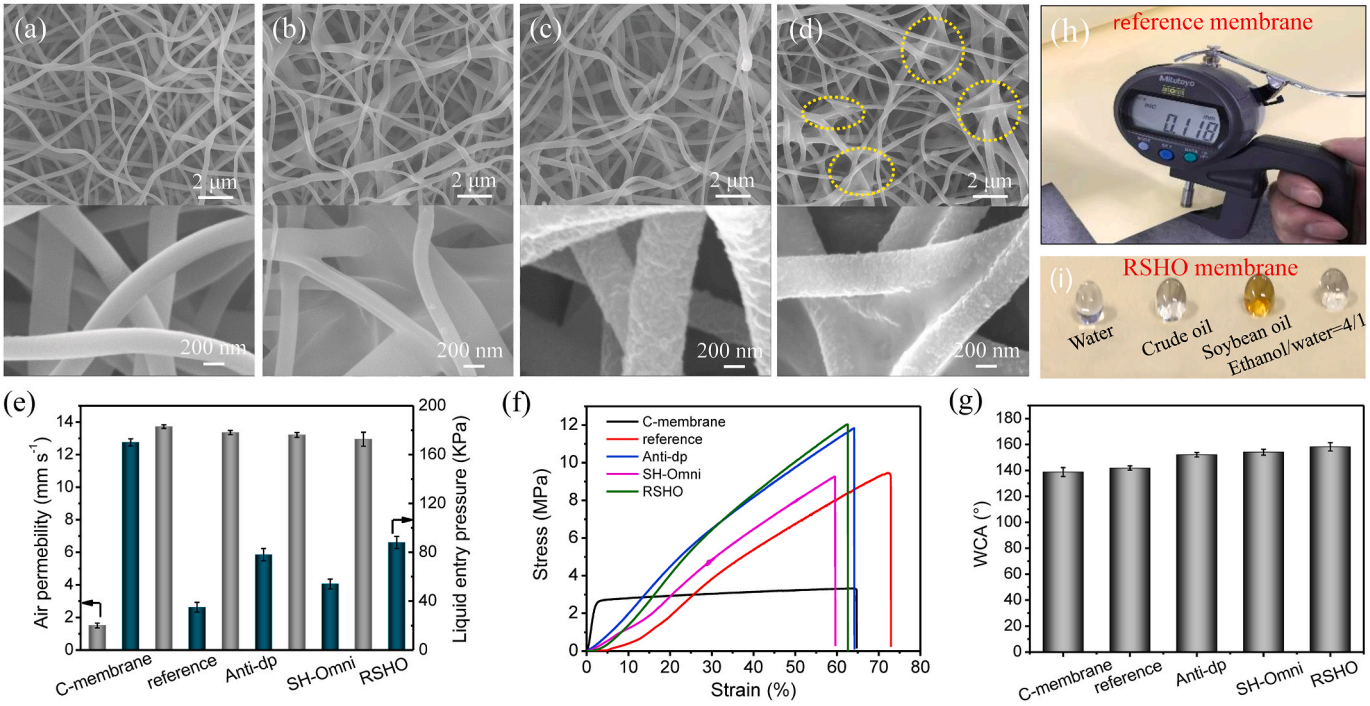

Fig. 2. FE-SEM images of (a) the reference membrane, (b) the Anti-dp membrane, (c) the SH-Omni membrane and (d) the RSHO membrane. (e) The air permeability and the liquid entry pressure, (f) the mechanical strength and (g) the surface wettability of relevant membranes. (h) Optical images showing the membrane thickness. (i) Photographic images of different liquid droplets on the RSHO membrane surface.

the fibers of the fibrous membrane with PDMS (Anti-dp membrane), not only induced more robust pore structure (Fig. 2b), increasing its LEP, but there was no apparent pore blockage, thus negligibly decreasing the air permeability by only ~2.62% (Fig. 2e).

As LEP is also dependent upon the surface wetting properties of the membrane, we confirmed that the enhancement LEP of the fibrous membrane was attributed to the PDMS welding fibers and the improvement in membrane hydrophobicity by grafting of fluorinated silica nanoparticles (Fig. 2e). For example, while the LEP increased by 122.85% after welding the fibrous membrane with PDMS (Anti-dp membrane), the LEP increased by 54.28% after grafting fluorinated silica nanoparticles to the fibrous membrane (SH-Omni membrane). The combined effect of PDMS welding and increased hydrophobicity via grafting of fluorinated silica nanoparticles to the fibrous membrane (RSHO membrane) resulted in a 151.42% increase in LEP compared the reference fibrous membrane. Furthermore, the air permeability of the RSHO membrane (12.95 mm s^{-1}) is only slightly lower than that of the reference membrane (13.72 mm s^{-1}), indicating that the membrane surface modification techniques did not significantly hinder the membrane's permeability to gaseous components such as water vapor. This result further supports that the PDMS welded fibers in the Anti-dp and RSHO membranes effectively enhances the membranes' resistance to wetting via hydraulic perturbance as compared to the randomly stacked fibers with weak interactions in the reference and SH-Omni membranes [41].

To further assess the fabricated membranes' ability to resist wetting via hydraulic perturbance, their mechanical properties were measured to elucidate the individual membrane's ability to resist pore deformation under stress (Fig. 2f). The C-membrane exhibited a linear stress-strain curve with little elongation (2.82%) under a small stress up to 2.66 MPa, at which point the material began to fail. All of the fibrous membranes presented similar, nonlinear, stress-strain curves with little elongation (0–~13%) under small stress (0–2 MPa), followed by a large elongation (~13–73%) when increasing the stress until material failure [42,43]. The distinct differences in elongation under stress between the C-membrane fabricated via phase inversion and fibrous membranes displays the deformable nature of fibrous membrane pores. Even so, the Anti-dp and RSHO membranes display a similar maximum stress of ~12 MPa, which is higher than that of both the reference and SH-Omni membranes of about 9 MPa. The improved mechanical strength of the Anti-dp and RSHO membranes can be attributed to the PDMS-welded intersecting fibers. Meanwhile, the maximum strain of the Anti-dp and RSHO membranes (~63–64%) was lower than that of the reference membrane (~73%). Young's modulus of relevant membranes was also used to uncover the resistance of membrane pore deformation, as shown in Fig. S3. The C-membrane displays a high Young's modulus of 1821 MPa, owing to its closed and welding pore structure while the Young's modulus of RSHO membrane is increased from 67 to 238 MPa. These measurements demonstrated that the welding technique was beneficial for resisting membrane pore deformation and, to some extent, reducing the impact of asymmetric disturbation of feed/permeate flow rate on enlarging membrane pores.

To further investigate the membrane's surface wetting properties, the static water contact angles (WCA) were quantified (Fig. 2g). The WCA of the C-membrane and reference membrane were relatively similar, at 139° and 142°, respectively, while the WCA of PDMS welded fibrous membrane (Anti-dp membrane) is increased to 152°. This can likely be attributed to the lower surface energy of PDMS in the Anti-dp membrane compared to the polyimide in the reference membrane and PVDF in the C-membrane as well as the slightly rougher surface morphology imparted by the stacked fibers. The SH-Omni membrane shows similar wetting properties to the Anti-dp membrane with WCA of 154° where the increase in WCA compared to the reference membrane can be attributed to the roughness imparted by grafting silica nanoparticles and ultra-low surface energy 17-FAS. Ultimately, the RSHO membrane exhibits a WCA of 158°, where the overall increase in WCA compared to that of the reference membrane can be attributed to the synergistic effects of the hydrophobic PDMS coating onto the polyimide fibers, the surface roughness imparted by the adsorbed silica nanoparticles, and the ultralow-surface-energy 17-FAS grafted to the silica nanoparticles via well-established silane chemistry [44,45]. For fair comparison of membrane properties and how they relate to wetting

resistance and other membrane performance metrics such as water vapor flux, the commercial membrane fabricated via phase inversion (C-membrane) and the reference fibrous membrane with different modifications (the substrate for the Anti-dp, SH-Omni, and RSHO fibrous membranes) were chosen due to their similar thicknesses, 120 ± 2 μm and 118 ± 3 μm, respectively, as shown in Fig. 2h. More importantly, the RSHO membrane exhibits robust omniphobicity, resisting wetting by low-surface-tension liquids such as crude oil, soybean oil and ethanol/water mixture (Fig. 2i) which wetted the C-membrane immediately.

3.2. Resistance to scale-induced wetting

(i) Long-term resistance to wetting by NaCl. To compare the long-term resistance to scale-induced wetting between phase-inversion and electrospun fibrous membranes, the C-membrane and the reference membrane were used in DCMD experiments (Fig. S4) with constant feed concentrations of 3.5, 10, and 20 wt% NaCl (Figs. S5 and S6). While at each NaCl concentration the initial water vapor flux of the reference membrane was greater than that of the C-membrane, the reference membrane was more prone to scaling and the subsequent scale-induced wetting, especially with the 10 and 20 wt% NaCl feed solutions [23,46,47]. Post-experiment FE-SEM images of the C-membrane reveal no apparent scaling crystals, but the EDX mapping shows small scale deposits are spread over the membrane surface (Fig. S5b), explaining the slight decrease in water vapor flux in the 10 and 20 wt% NaCl experiments. FE-SEM images of the reference membrane (Fig. S6 (b-d)) reveal that with increasing initial NaCl feed concentration, scaling crystal size increased, which increased the rate of membrane pore blockage and subsequent crystal penetration into the membrane pores. This increased rate of crystal deposition and/or growth resulted in the continuous decline in water vapor flux and increase in distillate stream conductivity.

To explore the effect of the robust pore structure induced via PDMS welding and the increased hydrophobicity via grafting and fluorinating silica nanoparticles on the fibrous membranes' MD performance, the membranes were used in long-term DCMD experiments with constant feed concentrations of 20 wt% NaCl. Although the membranes demonstrated above exhibit excellent scaling and wetting resistance against low concentration (3.5 and 10 wt%) NaCl feed solutions (Fig. S5-8), the scaling and wetting resistance of the reference, Anti-dp, and SH-Omni membranes are inferior to that of the RSHO membrane when subjected to high-salinity (20 wt%) NaCl feed solution (Fig. 3). This result demonstrates that the synergistic effects of the anti-deformable pores, induced by PDMS welding, and the superhydrophobic-omniphobic surface, induced by grafting and fluorinating silica nanoparticles, are indispensable for long-term scaling and scale-induced wetting resistance for fibrous membranes used to concentrate high-salinity feed solutions [31,48–50]. Interestingly, both the C-membrane and the RSHO membrane exhibited excellent scaling and scale-induced wetting resistance after 24 h of operation. This phenomenon observed for the C-membrane may be attributed to its small average pore size, anti-deformable pores, as well as dense membrane structure. However, the water vapor flux of the RSHO membrane is about 2.3 times higher than that of the C-membrane and thus the RSHO membrane's MD performance is superior overall.

(ii) Resistance to wetting when concentrating model high salinity solution. To compare the resistance to scale-induced wetting when concentrating a high-salinity feed solution between the conventional phase-inversion membrane and the fabricated fibrous membrane, the C-membrane and RSHO membrane were used to concentrate an NaCl feed solution with an initial concentration of 20 wt% NaCl in DCMD experiments (Fig. 4 and S9). Herein, we intentionally chose 20 wt% NaCl as feed solution, which is approaching its saturation concentration, to reduce the experiment time. It is worth noting the approximately 2 times greater water vapor flux observed for the RSHO membrane compared to

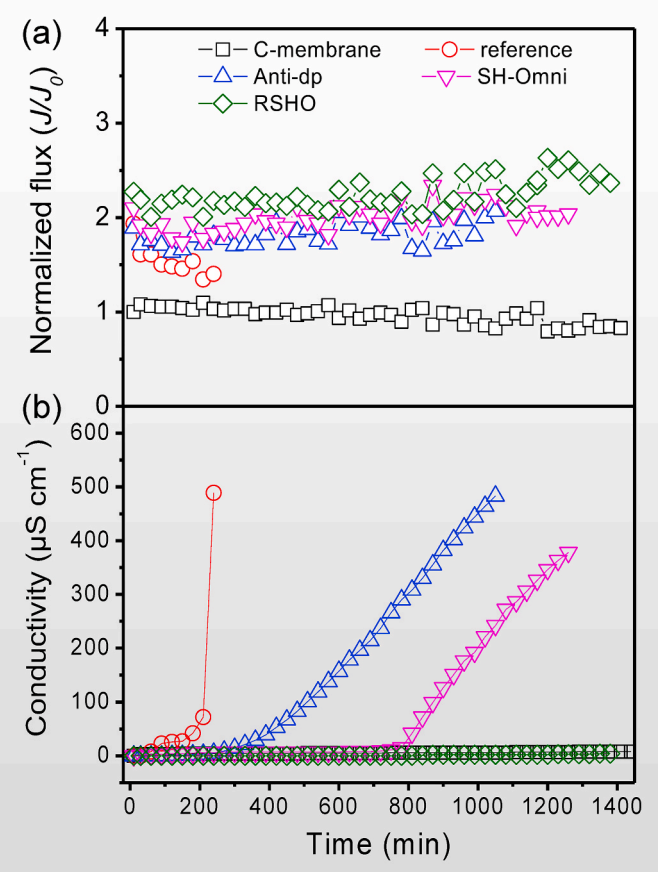

Fig. 3. DCMD performance (a) Normalized water flux and (b) Conductivity of the high salinity wastewater of relevant membranes for durable desalination of 20 wt% of NaCl solution. The initial water flux of the C-membrane, reference membrane, Anti-dp membrane, SH-Omni membrane, and RSHO membrane is 11.20, 21.70, 21.18, 23.55 and 25.48 L m^{-2} h^{-1}, respectively. (The initial volume of 20 wt% NaCl is 800 mL, both the flow rates of the feed and distillate were maintained at 100 mL min^{-1} (9.21 cm s^{-1} in our MD module), the temperate of the feed side and distilled side was fixed at 55 and 20 °C, respectively.).

that of the C-membrane (Fig. 4a). Most importantly, given the enhanced flux due to the unique interconnected pores of the RSHO membrane, 500 mL of distilled water can be recovered in 34 h while the C-membrane with closed pore structure should take about 60.5 h as shown in Fig. 4b, indicating that the RSHO membrane is more energy and time-efficient. Both membranes exhibit a gradual decrease in water vapor flux as the concentration of NaCl in the feed solution increased which, in part, can be attributed to the decline in vapor pressure, and thus driving force for water vapor transport, with increasing salt concentration [34]. The increase in distillate conductivity in the C-membrane experiment as shown in Fig. 4c indicates that the embedded scaling crystals grew into the membrane pores, creating a path for saline feed liquid to pass directly to the distillate while the RSHO membrane resisted scale induced wetting and thus maintained excellent salt rejection efficiency throughout the entire experiment (Fig. 4b). Additionally, FE-SEM images with corresponding elemental mapping of the RSHO membrane and C-membrane after concentrating the NaCl solution from 20 to 38 wt% reveal a scale layer composed of NaCl crystals with various sizes and geometries (Fig. 4d and Fig. S10). The layer of NaCl crystals are both deposited on the C-membrane surface and embedded in its pores, while only a small amount of NaCl crystals are observed on the RSHO membrane surface. The scaling, and subsequent scale-induced wetting, behavior of the C-membrane and the RSHO membrane depends on the membrane surfaces. The engineered roughness and ultra-low surface

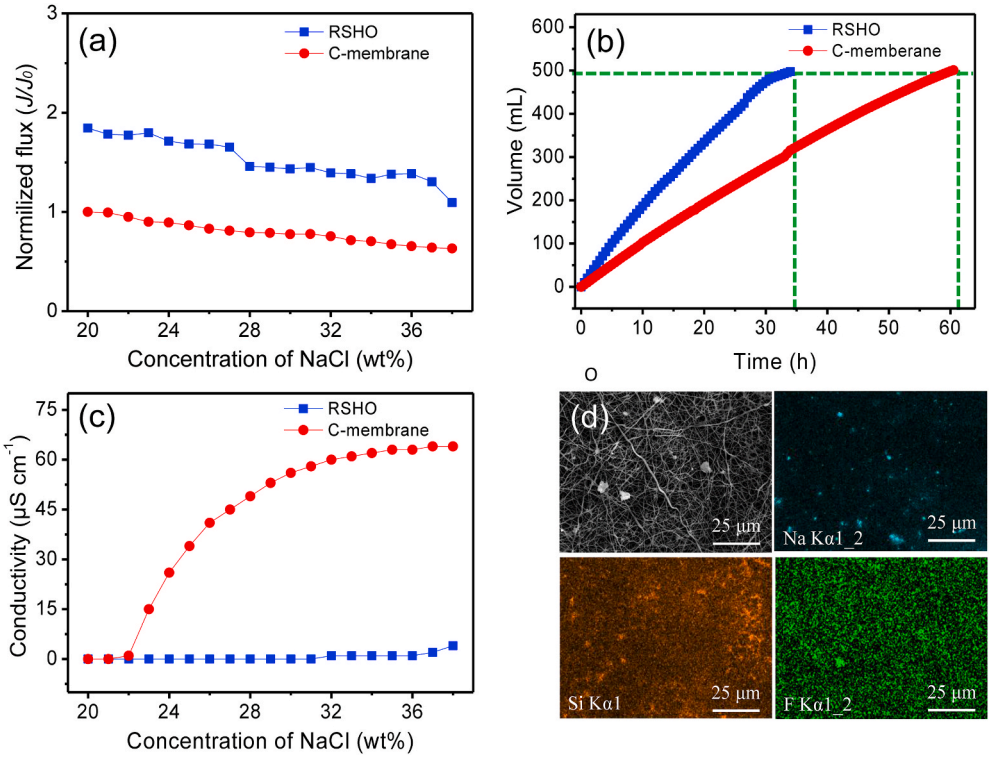

Fig. 4. Concentration performances of the C-membrane and the RSHO membrane for persistently concentrating the high salinity wastewater with an initial 20 wt% of NaCl feed solution. (a) Normalized flux as a function of the feed solution concentration and (b) the mass of collected distilled water as a function of the time. (c) Permeate conductivity of the above two membranes as a function of the feed solution concentration. (d) FE-SEM image of the RSHO membrane with corresponding elemental mapping images after concentrating NaCl solution from 20 to 38 wt%. The initial water flux of the C-membrane and RSHO membrane is 12.44 and 22.94 L m^{-2} h^{-1}, respectively. (The initial volume of 20 wt% NaCl is 800 mL, both the flow rates of the feed and distillate were maintained at 100 mL min^{-1} (9.21 cm s^{-1} in our MD module), the temperate of the feed side and distilled side was fixed at 55 and 20 °C, respectively.).

energy of the RSHO membrane allows it to maintain a stable Cassie-Baxter wetting state and thus avoid contact between the feed liquid and membrane surface via a stable air layer while the combined low surface energy effects of the PDMS and 17-FAS decrease the nucleation potential on the RSHO membrane surface [44,51,52].

(iii) Resistance to wetting when concentrating industrially relevant high-salinity solutions: reverse osmosis brine, gypsum, and calcium chloride. The RSHO membrane's ability to concentrate industrially relevant high-salinity salt solutions in DCMD was compared between reverse osmosis (RO) brine, gypsum, and calcium chloride feed solutions (Fig. 5). The RSHO membrane was able to effectively concentrate the RO brine and calcium chloride feed solutions suffering only a ~10% decline in water vapor flux as the feed concentration increased by 285%, thus decreasing the driving force for water vapor transport [34]. Furthermore, salt rejection efficiency of ~100% was maintained throughout the entire experiment. However, the RSHO membrane was less effective in concentrating the gypsum feed solution as it was both scaled and wetted after recovering ~210 mL of distillate. This phenomenon has been previously reported by Lin and Xiao, in that the superhydrophobic membrane cannot effectively eliminate gypsum scaling and scale-induced wetting long-term [4,18,23]. The fundamental differences in scaling and scale-induced wetting behaviors between feed solutions, specifically gypsum and NaCl, needs further investigation in order to develop effective mitigation strategies or novel membrane fabrication techniques that may resist gypsum scaling long-term.

3.3. Resistance to surfactant-induced wetting in high-salinity feed solutions

Although the C-membrane and the RSHO membrane displayed similar resistance to scaling and wetting when faced with single-component high-salinity NaCl feed solution, the conventional hydrophobic and superhydrophobic membranes used in MD generally fail to effectively separate high-salinity wastewater containing amphiphilic organic contaminants such as surfactants, especially in high concentration of 20 wt% NaCl. To compare the surfactant-induced wetting resistance of the RSHO membrane and C-membrane, 0.1 mM SDBS was used to model a typical amphiphilic contaminate in high-salinity (20 wt % NaCl) feed solution. As shown in Fig. 6, the RSHO membrane exhibited stable water vapor flux and high salt rejection efficiency throughout the entire experiment (1440 min), while the C-membrane was almost immediately wetted, with continuously increasing conductivity from the beginning of the experiment to 491 μS cm^{-1} after 420 min. It is worth noting that the SH-Omni membrane can resist surfactant-induced wetting in saline feed solutions according to previous study [23], but it fails to effectively resist scale-induced wetting in the presence of high-salinity NaCl feed solution (20 wt%) (Fig. S7). These results demonstrate that the synergistic effects of anti-deformable pores and low-surface-energy surface chemistry plays a key role in high performance MD for fibrous membranes with both surfactant and scaling-induced wetting resistance while maintaining superior water vapor flux characteristics relative to conventional phase inversion membranes.

3.4. Insight into the anti-wetting mechanism with the RSHO membrane

In the crossflow DCMD system (Fig. S4), with the membrane sandwiched between the flowing feed and distillate streams, the membrane element continuously vibrated. In the case of membrane vibration as shown in Video S1, the water flow produces a non-vertical impact force on the membrane, generating an expanding effect on the membrane pore (Fig. S11). To investigate the anti-scaling and anti-wetting effect of the anti-deformable pores in the RSHO membrane, ABAQUS software was used to simulate the pore deformation. First, the pore deformation effect was simulated for comparing the PDMS welding effect between the reference and Anti-dp membranes in flowing water. In the simulation experiment, all the fibers were assumed to be cylindrical structures with equal diameter. The pore deformation ratio of the reference membrane is about 100 times higher than that of the RSHO membrane that calculated by the ABAQUS software. If the fibrous membrane had not been welded, the saline water would contact the air-layer inside the membrane pores (inset in Fig. 7a). This provides the opportunity for

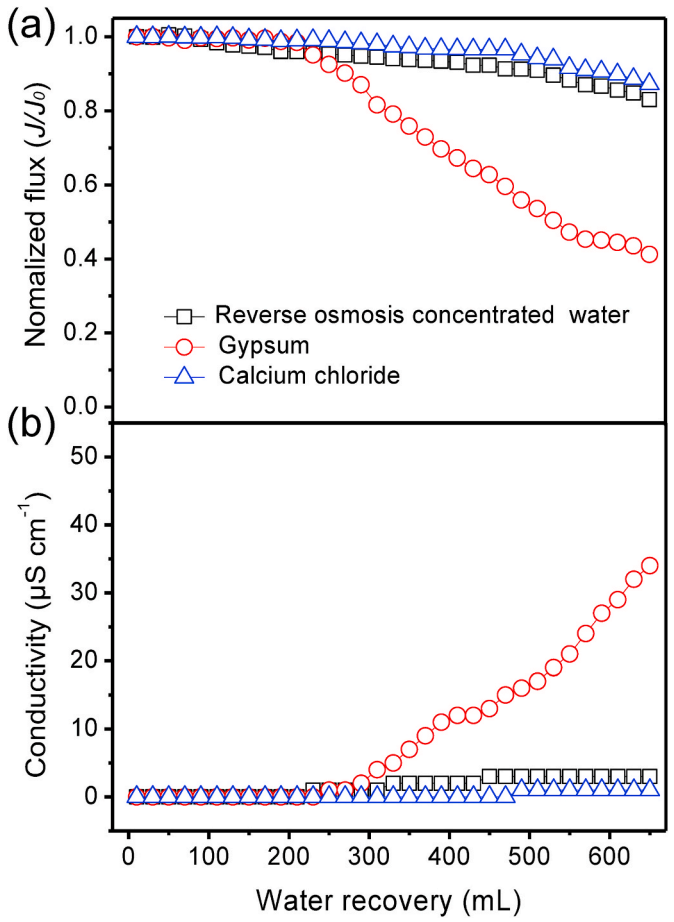

Fig. 5. Normalized flux and distillate conductivity as a function of the water recovery using the RSHO membrane in reverse osmosis concentrated water, gypsum and calcium chloride scaling and wetting experiments, respectively. The average initial water flux for concentrating the three types of salt solution is 30.52, 34.95 and 35.55 L m^{-2} h^{-1}. The reverse osmosis concentrated water was composed of 32.61 g L^{-1} NaCl, 1.03 g L^{-1} KCl, 4.52 g L^{-1} $MgCl_2$, 2.91 g L^{-1} $MgSO_4$ and 1.80 g L^{-1} $CaSO_4$. The gypsum was composed of 14 mM L^{-1} $CaCl_2$ and 14 mM L^{-1} Na_2SO_4. The feed $CaCl_2$ concentration was fixed at 1.5 wt%. (The initial volume of simulated RO concentrated water, gypsum water, and calcium chloride water is 958, 996.45 and 998.85 mL, respectively, both the flow rates of the feed and distillate were maintained at 100 mL min^{-1} (9.21 cm s^{-1} in our MD module), the temperate of the feed side and distilled side was fixed at 55 and 20 °C, respectively.).

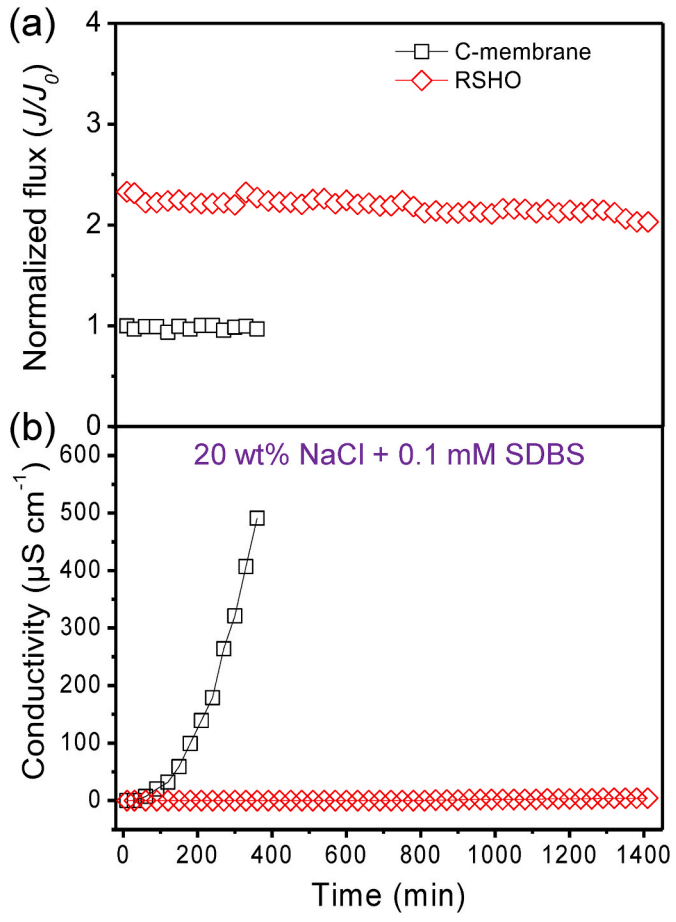

Fig. 6. Desalination performances of the high salinity wastewater of relevant membranes for durable desalination of 20 wt% of NaCl solution with 0.1 mM of SDBS. The initial water flux of the C-membrane and RSHO membrane is 10.95 and 25.22 L m^{-2} h^{-1}, respectively. (The initial volume NaCl + SDBS solution is 800 mL, both the flow rates of the feed and distillate were maintained at 100 mL min^{-1} (9.21 cm s^{-1} in our MD module), the temperate of the feed side and distilled side was fixed at 55 and 20 °C, respectively.).

saline water to penetrate the membrane pores and gradually pave free diffusion of salt molecules from the concentrated feed side to the distillate side. This guess can be verified by the experiment that the reference membrane was filled with saline water under occasional situation as shown in Fig. S12. Instead, the Anti-dp membrane maintains robust pore stability allows the fibrous membrane to overcome the asymmetrical hydraulic perturbance that enlarges membrane pore size thus, stabilizing the surface-bound air layer for long-term scaling resistance (Fig. 7b).

Supplementary data related to this article can be found at https://doi.org/10.1016/j.memsci.2020.118768.

Other than establishing anti-deformable pores, surface wettability is also an essential factor for improving fibrous membrane wetting resistance because the surface roughness and surface free energy play a pivotal role in determining the stability of the air-layer in the membrane pores (Fig. S13) [23]. Hence, membrane superhydrophobicity and omniphobicity further enhances the anti-deformable pore fibrous membrane's ability to resist wetting. Generally speaking, roughness is known to increase the hydrophilicity of a high surface energy surface or

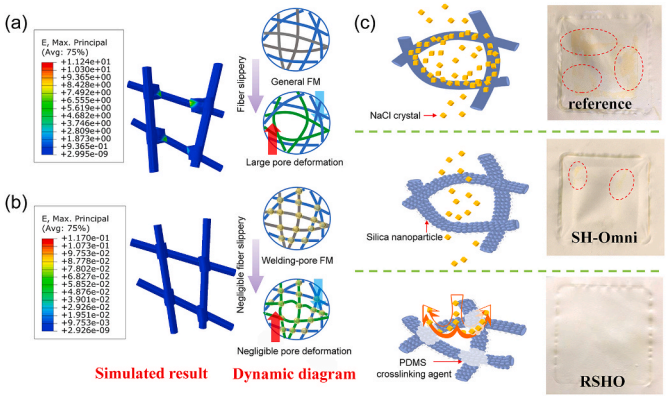

Fig. 7. ABAQUS software was used to simulate the ability of different pore structured membranes to resist membrane pore deformation, (a) the reference membrane and (b) the RSHO membrane. (c) Schematic demonstrating the membrane surfaces wettability and pore structure on the effect of membrane anti-scaling performance.

increase hydrophobicity of a low surface energy surface [53,54]. Therefore, given the same intrinsic surface free energy, a smooth hydrophobic membrane can be more easily wetted than a hierarchically

rough hydrophobic membrane surface. Additionally, the hierarchically rough membrane surface would be endowed with a large number of small protrusions that trap air underneath the liquid droplet, achieving a metastable Cassie-Baxter wetting state. The existence of the Cassie-Baxter wetting state results in a stabile surface-bound air layer that reduces contact between the membrane surface and high-salinity feed solution, scaling crystals, and feed solutions with amphiphilic components to limit the potential for wetting altogether.

The improved liquid entry pressure of the RSHO membrane demonstrated in also reveals the synergistic wetting resistance effect of the anti-deformable pores and enhanced surface wettability of the fibrous membrane. However, the inclusion of the cross-linked PDMS and the fiber welding at their junctions may potentially smooth the membrane surface roughness and decrease the membrane hydrophobicity (Figs. S14 and 15). With lower PDMS/17-FAS concentrations (0.5–1.0 wt%), anti-deformable pores and rough fiber surfaces could be observed while the WCA increased from 154 to 158°. Further increasing the PDMS/17-FAS concentration up to 3 wt% decreased the fiber surface roughness and thus decreased the WCA to 152° [55]. Meanwhile, the RSHO membrane's wetting resistance also depended on the concentrations of PDMS/17-FAS (Fig. S16), demonstrating that the higher PDMS/17-FAS concentrations (3 wt%) considerably compromises the wetting resistance of the fibrous membrane.

To better understand the scaling and wetting status of the C-membrane and the RSHO membrane after the DCMD experiment, both membranes were removed from the test cell and visually examined (Fig. 7c & Fig. S17). The feed side surface of the RSHO membrane and C-membrane remained clean of any visible scaling crystals, while a large area of scaling crystals was visible on both the reference and SH-Omni membrane surfaces (highlighted by the red dotted circles in Fig. 7c). For a smoother hydrophobic membrane surface, the membrane can be easily wetted because the increased probability of NaCl crystal deposition/nucleation and amphiphilic contaminant adsorption on the membrane surface (Fig. 7c). For the SH-Omni membrane surface, the stable air layer induced by the superhydrophobic membrane wetting properties effectively restricts direct contact between the membrane surface and the high-salinity, amphiphilic contaminant containing, feed solution and scale inducing salt crystals, thus, to some extent, effectively relieves crystal/amphiphilic contaminant deposition on the membrane surface. However, the hydraulic perturbation imposed on the membrane due to the water flow led to pore deformation and thus, provided an opportunity for NaCl crystals to embed into and wet the membrane pores. Fortunately, the RSHO membrane can stabilize the surface-bound air layer structurally and chemically, which not only alleviates the deformation of fibrous membrane pores but also avoids direct contact between the membrane surface and the scaling crystals or amphiphilic contaminants, empowering the long-term reliability of the superior water vapor flux fibrous membrane for concentration of high-salinity wastewaters.

4. Conclusion

In summary, a novel structured fibrous membrane with anti-deformable pores and superhydrophobic-omniphobic surface was developed via sequential electrospinning, membrane roughness enhancement, and inter-fiber welding to achieve a novel membrane with superior water vapor flux and reliable resistance to scaling and wetting. The membrane exhibited excellent scaling and wetting resistance along with comparably high water flux when concentrating high-salinity NaCl solution, simulated reverse osmosis brine, gypsum, and amphiphilic contaminant containing high-salinity wastewater. Based on the experimental results, the mechanism of the RSHO membrane's increased resistance to scaling and resistance to wetting by both organic and inorganic contaminants was discussed. The pore deformation effect caused by hydraulic perturbance on the membrane due to water flow was also revealed by ABAQUS software simulations. The synergistic effect of the anti-deformable pores and the superhydrophobic-omniphobic surface wetting properties of the fibrous membrane allows for the durable concentration of high-salinity wastewaters, paving a novel methodology with well-defined theory to control wetting of fibrous membrane for the treatment of high-salinity wastewaters.

Credit author statement

Zhigao Zhu: Conceptualization, Investigation, Methodology, Data curation, Writing–original draft, Writing–review & editing. **Lingling Zhong**: Investigation, Methodology, Visualization. **Thomas Horseman**: Formal analysis, Writing–review & editing. **Zhiyuan Liu**: ABAQUS simulation. **Gaofeng Zeng**: Characterization. **Zhenyu Li**: Characterization. **Shihong Lin**: Conceptualization, Formal analysis, Writing–review & editing. **Wei Wang**: Conceptualization, Methodology, Funding acquisition, Writing–review & editing, Supervision.

Declaration of competing interest

The authors declare that they have no known competing financial interests or personal relationships that could have appeared to influence the work reported in this paper.

Acknowledgments

The authors gratefully acknowledge the National Natural Science Foundation of China (Nos. 52000105 and 51873047), the Natural Science Foundation of Jiangsu Province (No. BK20200478), the 67th batch of China Postdoctoral Science Foundation (No. 2020M671503), the Scientific Research Foundation of Heilongjiang Prov. (No. YQ2020B003), the Key Laboratory of Low-Carbon Conversion Science & Engineering, Shanghai Advanced Research Institute, Chinese Academy of Sciences (No. KLLCCSE-201906), the Applied Basic Research Program of Science and Technology Department of Sichuan Province (No. 2018JY0302).

Appendix A. Supplementary data

Supplementary data to this article can be found online at https://doi.org/10.1016/j.memsci.2020.118768.

References

[1] S. Jorfi, S. Ghafari, B. Ramavandi, R.D.C. Soltani, M. Ahmadi, Biodegradation of high saline petrochemical wastewater by novel isolated halotolerant bacterial strains using integrated powder activated carbon/activated sludge bioreactor, Environ. Prog. Sustain. Energy 38 (2018) 13088.
[2] V. Colla, T.A. Branca, F. Rosito, C. Lucca, B.P. Vivas, V.M. Delmiro, Sustainable reverse osmosis application for wastewater treatment in the steel industry, J. Clean. Prod. 130 (2016) 103–115.
[3] O. Lefebvre, R. Moletta, Treatment of organic pollution in industrial saline wastewater: a literature review, Water Res. 40 (2006) 3671–3682.
[4] V. Karanikola, C. Boo, J. Rolf, M. Elimelech, Engineered slippery surface to mitigate gypsum scaling in membrane distillation for treatment of hypersaline industrial wastewaters, Environ. Sci. Technol. 52 (2018) 14362–14370.
[5] J. Bundschuh, N. Ghaffour, H. Mahmoudi, M. Goosen, S. Mushtaq, J. Hoinkis, Low-cost low-enthalpy geothermal heat for freshwater production: innovative applications using thermal desalination processes, Renew. Sustain. Energy Rev. 43 (2015) 196–206.
[6] M. Qasim, M. Badrelzaman, N.N. Darwish, N.A. Darwish, N. Hilal, Reverse osmosis desalination: a state-of-the-art review, Desalination 459 (2019) 59–104.
[7] Z. Xiao, Z. Li, H. Guo, Y. Liu, Y. Wang, H. Yin, X. Li, J. Song, L.D. Nghiem, T. He, Scaling mitigation in membrane distillation: from superhydrophobic to slippery, Desalination 466 (2019) 36–43.
[8] R. Zhang, J. Tian, S. Gao, B. Van der Bruggen, How to coordinate the trade-off between water permeability and salt rejection in nanofiltration? J. Mater. Chem. A 8 (2020) 8831–8847.
[9] H.R. Golsefatan, M. Fazeli, A.R. Mehrabadi, H. Ghomi, Enhancement of corrosion resistance in thermal desalination plants by diamond like carbon coating, Desalination 409 (2017) 183–188.
[10] Q. Li, A. Omar, W. Cha-Umpong, Q. Liu, X. Li, J. Wen, Y. Wang, A. Razmjou, J. Guan, R.A. Taylor, The potential of hollow fiber vacuum multi-effect membrane distillation for brine treatment, Appl. Energy 276 (2020), 115437.

[11] I.B. Onyeachu, M.M. Solomon, S.A. Umoren, I.B. Obot, A.A. Sorour, Corrosion inhibition effect of a benzimidazole derivative on heat exchanger tubing materials during acid cleaning of multistage flash desalination plants, Desalination 479 (2020), 114283.
[12] C. Cuviella-Suárez, A. Colmenar-Santos, D. Borge-Diez, Á. López-Rey, Heat recovery in sanitary-ware industry applied to water and energy saving by multi-effect distillation, J. Clean. Prod. 213 (2019) 1322–1336.
[13] G. Chen, R. Liu, H.K. Shon, Y. Wang, J. Song, X. Li, T. He, Open porous hydrophilic supported thin-film composite forward osmosis membrane via co-casting for treatment of high-salinity wastewater, Desalination 405 (2017) 76–84.
[14] A. Alkhudhiri, N. Darwish, N. Hilal, Membrane distillation: a comprehensive review, Desalination 287 (2012) 2–18.
[15] F. Kiefer, A. Praebst, K.S. Rodewald, T. Sattelmayer, Membrane scaling in vacuum membrane distillation-Part 1: in-situ observation of crystal growth and membrane wetting, J. Membr. Sci. 590 (2019), 117294.
[16] D.M. Warsinger, J. Swaminathan, E. Guillen-Burrieza, H.A. Arafat, J.H. Lienhard V, Scaling and fouling in membrane distillation for desalination applications: a review, Desalination 356 (2015) 294–313.
[17] T. Horseman, C. Su, K.S.S. Christie, S. Lin, Highly effective scaling mitigation in membrane distillation using a superhydrophobic membrane with gas purging, Environ. Sci. Technol. Lett. 6 (2019) 423–429.
[18] Z. Xiao, R. Zheng, Y. Liu, H. He, X. Yuan, Y. Ji, D. Li, H. Yin, Y. Zhang, X.M. Li, T. He, Slippery for scaling resistance in membrane distillation: a novel porous micropillared superhydrophobic surface, Water Res. 155 (2019) 152–161.
[19] Z. Wang, Y. Chen, F. Zhang, S. Lin, Significance of surface excess concentration in the kinetics of surfactant-induced pore wetting in membrane distillation, Desalination 450 (2019) 46–53.
[20] M. Rezaei, D.M. Warsinger, J.H. Lienhard V, W.M. Samhaber, Wetting prevention in membrane distillation through superhydrophobicity and recharging an air layer on the membrane surface, J. Membr. Sci. 530 (2017) 42–52.
[21] P. Lin, M. Yang, Y. Li, J. Chen, Prevention of surfactant wetting with agarose hydrogel layer for direct contact membrane distillation used in dyeing wastewater treatment, J. Membr. Sci. 475 (2015) 511–520.
[22] Z. Wang, Y. Chen, X. Sun, R. Duddu, S. Lin, Mechanism of pore wetting in membrane distillation with alcohol vs. surfactant, J. Membr. Sci. 559 (2018) 183–195.
[23] C. Su, T. Horseman, H. Cao, K. Christie, Y. Li, S. Lin, Robust superhydrophobic membrane for membrane distillation with excellent scaling resistance, Environ. Sci. Technol. 53 (2019) 11801–11809.
[24] Z. Wang, S. Lin, Membrane fouling and wetting in membrane distillation and their mitigation by novel membranes with special wettability, Water Res. 112 (2017) 38–47.
[25] A. Deshmukh, C. Boo, V. Karanikola, S. Lin, A.P. Straub, T. Tong, D.M. Warsinger, M. Elimelech, Membrane distillation at the water-energy nexus: limits, opportunities, and challenges, Energy Environ. Sci. 11 (2018) 1177–1196.
[26] R. Huang, Z. Liu, Y.C. Woo, W. Luo, S.R. Gray, M. Xie, Emerging investigator series: engineering membrane distillation with nanofabrication: design, performance and mechanisms, Environ. Sci.: Water Res. Technol. 6 (2020) 1786–1793.
[27] Z. Zhu, Z. Li, L. Zhong, R. Zhang, F. Cui, W. Wang, Dual-biomimetic superwetting silica nanofibrous membrane for oily water purification, J. Membr. Sci. 572 (2019) 73–81.
[28] X. An, G. Xu, B. Xie, Y. Hu, Structural tailoring of hierarchical fibrous composite membranes to balance mass transfer and heat transfer for state-of-the-art desalination performance in membrane distillation, J. Mater. Chem. A 7 (2019) 2376–2384.
[29] L. Deng, P. Li, K. Liu, X. Wang, B.S. Hsiao, Robust superhydrophobic dual layer nanofibrous composite membranes with a hierarchically structured amorphous polypropylene skin for membrane distillation, J. Mater. Chem. A 7 (2019) 11282–11297.
[30] Z. Zhu, L. Zhong, Y. Wang, G. Zeng, W. Wang, Mechanically durable biomimetic fibrous membrane with superhydrophobicity and superoleophilicity for aqueous oil separation, Chin. Chem. Lett. (2020), https://doi.org/10.1016/j.cclet.2020.1001.1038.
[31] C. Su, C. Lu, T. Horseman, H. Cao, F. Duan, L. Li, M. Li, Y. Li, Dilute solvent welding: a quick and scalable approach for enhancing the mechanical properties and narrowing the pore size distribution of electrospun nanofibrous membrane, J. Membr. Sci. 595 (2020), 117548.
[32] C. Su, C. Lu, H. Cao, K. Tang, J. Chang, F. Duan, X. Ma, Y. Li, Fabrication and post-treatment of nanofibers-covered hollow fiber membranes for membrane distillation, J. Membr. Sci. 562 (2018) 38–46.
[33] C. Boo, J. Lee, M. Elimelech, Omniphobic polyvinylidene fluoride (PVDF) membrane for desalination of shale gas produced water by membrane distillation, Environ. Sci. Technol. 50 (2016) 12275–12282.
[34] Z. Zhu, Y. Liu, H. Hou, W. Shi, F. Qu, F. Cui, W. Wang, Dual-bioinspired design for constructing membranes with superhydrophobicity for direct contact membrane distillation, Environ. Sci. Technol. 52 (2018) 3027–3036.
[35] Z. Zhu, L. Zhong, X. Chen, W. Zheng, J. Zuo, G. Zeng, W. Wang, Monolithic and self-roughened Janus fibrous membrane with superhydrophilic/omniphobic surface for robust antifouling and antiwetting membrane distillation, J. Membr. Sci. 615 (2020), 118499.
[36] S. Lin, S. Nejati, C. Boo, Y. Hu, C.O. Osuji, M. Elimelech, Omniphobic membrane for robust membrane distillation, Environ. Sci. Technol. Lett. 1 (2014) 443–447.
[37] X. Li, X. Yu, C. Cheng, L. Deng, M. Wang, X. Wang, Electrospun superhydrophobic organic/inorganic composite nanofibrous membranes for membrane distillation, ACS Appl. Mater. Interfaces 7 (2015) 21919–21930.
[38] J. Phattaranawik, Effect of pore size distribution and air flux on mass transport in direct contact membrane distillation, J. Membr. Sci. 215 (2003) 75–85.
[39] A.B.D. Cassie, S. Baxter, Wettability of porous surfaces, Trans. Faraday Soc. 40 (1944) 546–551.
[40] R.N. Wenzel, Resistance of solid surfaces to wetting by water, Ind. Eng. Chem. Res. 28 (1936) 988–994.
[41] B.S. Lalia, E. Guillen-Burrieza, H.A. Arafat, R. Hashaikeh, Fabrication and characterization of polyvinylidenefluoride-co-hexafluoropropylene (PVDF-HFP) electrospun membranes for direct contact membrane distillation, J. Membr. Sci. 428 (2013) 104–115.
[42] Z. Zhu, W. Wang, D. Qi, Y. Luo, Y. Liu, Y. Xu, F. Cui, C. Wang, X. Chen, Calcinable polymer membrane with revivability for efficient oily-water remediation, Adv. Mater. 30 (2018), e1801870.
[43] N. Sun, Z. Zhu, G. Zeng, Bioinspired superwetting fibrous skin with hierarchical roughness for efficient oily water separation, Sci. Total Environ. 744 (2020), 140822.
[44] C. Boo, J. Lee, M. Elimelech, Engineering surface energy and nanostructure of microporous films for expanded membrane distillation applications, Environ. Sci. Technol. 50 (2016) 8112–8119.
[45] J.J. Cras, C.A. Rowetaitt, D.A. Nivens, F.S. Ligler, Comparison of chemical cleaning methods of glass in preparation for silanization, Biosens, Bioelectron 14 (1999) 683–688.
[46] S. Meng, Y. Ye, J. Mansouri, V. Chen, Crystallization behavior of salts during membrane distillation with hydrophobic and superhydrophobic capillary membranes, J. Membr. Sci. 473 (2015) 165–176.
[47] M. Rezaei, D.M. Warsinger, V.J. Lienhard, M.C. Duke, T. Matsuura, W. M. Samhaber, Wetting phenomena in membrane distillation: mechanisms, reversal, and prevention, Water Res. 139 (2018) 329–352.
[48] M.N. Kavalenka, F. Vullers, S. Lischker, C. Zeiger, A. Hopf, M. Rohrig, B.E. Rapp, M. Worgull, H. Holscher, Bioinspired air-retaining nanofur for drag reduction, ACS Appl. Mater. Interfaces 7 (2015) 10651–10655.
[49] D.J. Babu, M. Mail, W. Barthlott, J.J. Schneider, Superhydrophobic vertically aligned carbon nanotubes for biomimetic air retention under water (Salvinia Effect), Adv. Mater. Interfaces 4 (2017), 1700273.
[50] Y. Chen, K.J. Lu, T.-S. Chung, An omniphobic slippery membrane with simultaneous anti-wetting and anti-scaling properties for robust membrane distillation, J. Membr. Sci. 595 (2020).
[51] N.G.P. Chew, Y. Zhang, K. Goh, J.S. Ho, R. Xu, R. Wang, Hierarchically structured Janus membrane surfaces for enhanced membrane distillation performance, ACS Appl. Mater. Interfaces 11 (2019) 25524–25534.
[52] H. Attia, D.J. Johnson, C.J. Wright, N. Hilal, Robust superhydrophobic electrospun membrane fabricated by combination of electrospinning and electrospraying techniques for air gap membrane distillation, Desalination 446 (2018) 70–82.
[53] S. Gao, J. Sun, P. Liu, F. Zhang, W. Zhang, S. Yuan, J. Li, J. Jin, A robust polyionized hydrogel with an unprecedented underwater anti-crude-oil-adhesion property, Adv. Mater. 28 (2016) 5307–5314.
[54] A.K. An, J. Guo, E.-J. Lee, S. Jeong, Y. Zhao, Z. Wang, T. Leiknes, PDMS/PVDF hybrid electrospun membrane with superhydrophobic property and drop impact dynamics for dyeing wastewater treatment using membrane distillation, J. Membr. Sci. 525 (2017) 57–67.
[55] J. Sheng, Y. Xu, J. Yu, B. Ding, Robust fluorine-free superhydrophobic amino-silicone oil/SiO_2 modification of electrospun polyacrylonitrile membranes for waterproof-breathable application, ACS Appl. Mater. Interfaces 9 (2017) 15139–15147.